IEEE Access
Multidisciplinary | Rapid Review | Open Access Journal

Received September 20, 2019, accepted October 7, 2019, date of publication October 15, 2019,
date of current version November 6, 2019.

*Digital Object Identifier 10.1109/ACCESS.2019.2947439*

# Towards a Combination of Low Rank and Sparsity in EIT Imaging

**QI WANG, FEI LI, JIANMING WANG, XIAOJIE DUAN, AND XIUYAN LI**
Tianjin Key Laboratory of Optoelectronic Detection Technology and Systems, Tianjin Polytechnic University, Tianjin 300160, China
School of Electronics and Information Engineering, Tianjin Polytechnic University, Tianjin 300160, China

Corresponding author: Jianming Wang (wangjianming@tjpu.edu.cn)

This work was supported in part by the National Natural Science Foundation of China under Grant 61872269, Grant 61601324, and Grant 61903273, in part by the Natural Science Foundation of Tianjin Municipal Science and Technology Commission under Grant 18JCYBJC85300, in part by the Tianjin Enterprise Science and Technology Correspondent Project under Grant 18JCTPJC61600, in part by the Graduate Science and Technology Innovation Projects of Tianjin Polytechnic University under Grant 18129, and in part by the Tianjin Science and Technology Program under Grant 19PTZWHZ00020.

**ABSTRACT** Electrical impedance tomography (EIT) calculates the internal conductivity distribution of a body using electrical contact measurement and has become increasingly attractive in the biomedical field. However, the design of optimal tomography image reconstruction algorithms has not achieved an adequate level of progress and maturity. The spatial-temporal properties are crucial for the improvement of reconstruction quality and efficiency in dynamic EIT reconstruction. However, these properties have not been fully utilized in previous research. In this paper, a mathematical model for EIT reconstruction is built upon a combination of the low-rank and the sparsity theories. In addition to the low-rank method based on the nuclear norm constraint, the patch-based sparse method is also used to obtain the spatial features of a reconstructed image, according to the characteristic of an irregular boundary for the EIT image. The mathematical model of the new method is solved using the variable split (VS) algorithm. The imaging results are compared with the reconstruction results of the traditional algorithms. The experimental results demonstrate better performance of the new method compared with the traditional methods. The effectiveness of the proposed scheme is verified.

**INDEX TERMS** Dynamic image reconstruction, electrical impedance tomography, low-rank, sparsely, spatial-temporal.

## I. INTRODUCTION

Electrical impedance tomography (EIT) has been investigated extensively during past decades as a visualization and measurement technique, which can be used to obtain the image of the cross-sectional area without any interventions in the object body. Based on the theory that different media have different impedances, we can recover the interior impedance from the simultaneous measurements of the voltage or current on the boundary. EIT technology has the advantages of portability, safety, low-cost, noninvasiveness and rapid response [1], [2]. EIT is an attractive medical imaging technology with potential clinical application. However, maintaining high resolution in space together with low costs is still challenging [3], [4].

Due to the diffusive nature of EIT and the ill-posedness of the inverse imaging problem, the quality of reconstruction is often modest in comparison with that of many other imaging modalities [5]. Thus it is still of great interest to develop improved reconstruction algorithms that capable of yielding sufficiently useful information about the data. Recently, low-rank matrix reconstruction has drawn more attention to the image reconstruction area, which has also been used for EIT dynamic reconstruction [6], [7]. It exploits the spatial-temporal properties of dynamic reconstruction objects that are crucial for the improvement of reconstruction quality. Nuclear norm minimization has always been used to solve low-rank problem [7]. However, the spatial characteristics of each frame are not considered, so that partial feature information loss may occur, which could degrade the image quality. As a result, the final clinical diagnosis will be affected [4]. Thus, it is crucial to improve the low-rank method so that the spatial resolution of the EIT image can be further improved.

Compared with the low-rank method, a sparse strategy can resolve local features of the image [8]–[10]. The TV method has always been used for sparse reconstruction in

The associate editor coordinating the review of this manuscript and approving it for publication was Ge Wang.

these methods [11]–[13]. Although better image quality can be obtained, it is only suitable for an imaging field with a regular shape, e.g., a square image. However, the object field of EIT depends on the position of electrodes, which is always irregular. These methods are also not suitable for EIT image boundaries as the electrode position changes. Thus, how to build rational and powerful EIT reconstruction models is still a worthy research issue.

In this paper, we propose a low-rank plus sparse scheme for EIT imaging. For the low-rank part, we use a nuclear norm constraint. For the sparse part, we replace the global sparsity method with the patch-based sparsity method to meet the requirement of an irregular image boundary and to improve the spatial resolution of reconstructed image.

The ADMM algorithm is used to solve the low-rank plus sparse EIT model in this paper [14]–[16]. The simulation and experimental results are both provided.

## II. EIT RECONSTRUCTION

The dynamic EIT measurements correspond to the conductivity distribution can be approximated as

$$V = U(\sigma; I) = R(\sigma)I \tag{1}$$

where $U(\cdot)$ is the forward model mapping the conductivity distribution $\sigma$ and injected current vector $I$ to the boundary voltage vector $V$ and $R(\sigma)$ is the model mapping $\sigma$ to resistance.

We denote the spatio-temporal conductivity signal $\sigma(x, t)$, where $x$ is the spatial location and $t$ denotes time. In dynamic imaging applications, the temporal profiles of the pixels are indicated by the n-dimensional vector

$$q_i = [\sigma(x_i, t_0), \sigma(x_i, t_1), \cdots, \sigma(x_i, t_{l-1})]^T; \quad i = 0, \cdots, n-1 \tag{2}$$

where $n$ is the number of pixels in the reconstructed image and $l$ is the number of temporal samples. The spatial-temporal signal $\sigma(x, t)$ can be rearranged in a matrix form to exploit the correlations

$$\delta\sigma = \begin{bmatrix} \sigma(x_0, t_0) & \cdots & \sigma(x_0, t_{l-1}) \\ \vdots & & \\ \sigma(x_{n-1}, t_0) & & \sigma(x_{n-1}, t_{l-1}) \end{bmatrix} \tag{3}$$

The columns of $\delta\sigma \in R^{n\times l}$ correspond to the pixels of each two-dimensional image (conductivity distribution). The inverse problem is also called image reconstruction. If changes in conductivity are small, the inverse problem can be solved with sufficient accuracy by considering the linearized equation system

$$\delta U = U'(\sigma_0)\delta\sigma = J\delta\sigma \tag{4}$$

where $\delta U \in R^{m\times l}$(m is the number of independent voltage measurements) is the perturbation of boundary voltage due to the change of $\sigma$ and $J \in R^{m\times n}$ is the Jacobian matrix, that is the partial derivatives of voltages with respect to the conductivity.

## III. PROBLEM FORMULATION

In this section, we present the proposed mathematical model that is aimed to provide efficient accelerated EIT.

To exploit the sparsity and low-rank properties of the matrix. We formulate the problem as

$$\begin{aligned} \delta\sigma^* &= \arg\min_{\delta\sigma} \|J\delta\sigma - \delta U\|_2^2 \\ &s.t\ \mathrm{rank}(\delta\sigma) \le r, \quad \|D\delta\sigma\|_1 \le K \end{aligned} \tag{5}$$

where $r \le \min(m, l)$ is the rank constraint, $K$ is the sparsity constraint defined by the number of nonzero entries in sparse coefficients.

Rewriting the above constrained optimization problem using Lagrange's multipliers and relaxing the penalties, we obtain

$$\delta\sigma^* = \arg\min_{\delta\sigma} \|J\delta\sigma - \delta U\|_2^2 + \lambda_1 L(\delta\sigma) + \lambda_2 S(\delta\sigma) \tag{6}$$

where $L(\delta\sigma)$ represents the low-rank penalty function and $S(\delta\sigma)$ represents the sparse penalty function. $\lambda_1$ and $\lambda_2$ are regularization parameters. We use nuclear norm function, which is specified by

$$L(\delta\sigma) = \|\delta\sigma\|_* = \sum_{i=1}^{\min\{m,n\}} \sigma_i \tag{7}$$

where $\delta\sigma = U\Sigma V^*$ is the singular value decomposition of $\delta\sigma$ and $\Sigma = diag([\sigma_0, \sigma_1, \ldots \sigma_{r-1}])$ [18]. The operator $\|\cdot\|_*$ is the nuclear norm.

In this paper, the patch-based sparse method is used for sparse representation to obtain the local feature of reconstructed image and to meet the requirement of the irregular boundary problem of EIT [18]. The sparse penalty function $S(\delta\sigma)$ in equation (6) can be represented as

$$S(\delta\sigma) = \left\|D\alpha^i\right\|_1 \tag{8}$$

$$\min_{D,\Gamma} \sum_i \left\|P^i\delta\sigma - D_i\alpha^i\right\|_2^2$$

$$\text{s.t.} \ \left\|\alpha^i\right\|_0 \le T_0 \quad i = 1, \ldots, k \tag{9}$$

where $P^i \in R^{n\times L}$ defines the patch, and the $i$ th patch $\delta\sigma^i \in R^L$ is expressed as $\delta\sigma^i = P^i\delta\sigma$. $D$ is the sparse dictionary, which is composed of different patches. The K-SVD algorithm is used to learn the dictionary $D_i$ of the $i$ th patch. We define the combined dictionary $D = \begin{bmatrix} D_1 \\ D_2 \\ \vdots \\ D_k \end{bmatrix}$, $D \in R^{d\times d}$, where the sample is $d$ dimension, the sparse representation is $i$ dimension and the $k$ variable refers to $k$ block. $\Gamma$ is used to denote the set $\{\alpha_i\}_i$ of sparse representations of all patches. In problem (9), an initial dictionary $D_0$ is required for K-SVD learning [19]. Available initializations involve analytical dictionaries, such as wavelets and the discrete cosine transformation (DCT) matrix, or the training data themselves. In the paper, the DCT matrix is selected.

### A. OPTIMIZATION ALGORITHM

We introduce a novel variable splitting algorithm for the efficient recovery of the matrix using (6). We pose the regularized matrix recovery scheme as a constrained minimization problem using variable splitting [17]

$$\delta\sigma^* = \arg\min_{\delta\sigma} \|J\delta\sigma - \delta U\|_2^2 + \lambda_1 \mathrm{L}(R) + \lambda_2 \|S\|_1 \quad s.t\ \delta\sigma = R, \quad S = \delta\sigma; \tag{10}$$

where, $R$ and $S$ are auxiliary variables, which are also determined during the optimization process. We solve (11) using the penalty method, in which we minimize

$$G(\eta_1, \eta_2)(\delta\sigma, R, S) = \arg\min_{\delta\sigma} \|J\delta\sigma - \delta U\|_2^2 + \lambda_1 L(R) + \lambda_2 \|S\|_1 + \frac{\eta_1}{2}\|\delta\sigma - R\|_2^2 + \frac{\eta_2}{2}\|\delta\sigma - S\|_2^2 \tag{11}$$

where $\eta_1$ and $\eta_2$ are regularization parameters. Problem (11) is solved using an alternating minimization procedure.

$$\delta\sigma^{c+1} = \arg\min_{\delta\sigma} \|J\delta\sigma - \delta U\|_2^2 + \frac{\eta_1}{2}\|\delta\sigma - R\|_2^2 + \frac{\eta_2}{2}\|\delta\sigma - S\|_2^2 \tag{12}$$

$$R^{c+1} = \arg\min_{R} \left\|\delta\sigma^{c+1} - R\right\|_2^2 + \frac{2\lambda_1}{\eta_1}\mathrm{L}(R) \tag{13}$$

$$S^{c+1} = \arg\min_{S} \|\delta\sigma - S\|_2^2 + \frac{2\lambda_2}{\eta_2}\|S\|_1 \tag{14}$$

Similar alternating directions methods are widely used in compressed sensing and TV minimization [11], [12]. The first subproblem (12) is quadratic and hence can be solved analytically as

$$\delta\sigma^{c+1} = (J^T J + \frac{\eta_1}{2}Q^T Q)^{-1} \times (J^T \delta U + \frac{\eta_1}{2}R + \frac{\eta_2}{2}S) = \mathrm{T}(R, S) \tag{15}$$

where the operator $Q$ is defined as $Q(\delta\sigma) = D^*\delta\sigma$. This step can be solved efficiently by the conjugate gradient algorithm [20].

The second subproblem (13) is of a similar form of standard nuclear norm minimization problems. The iterative singular value thresholding (IST) scheme that is used in nuclear norm minimization can be generalized to the case that has nonconvex spectral penalties [20]. We would lead to obtain $R^{c+1}$ as a singular value thresholding of $\delta\sigma^{c+1}$, as specified by $S_{\lambda_1/\eta_1}$

$$R^{c+1} = (S_{\lambda_1/\eta_1} \circ \mathrm{T})(R^c, S^c) \tag{16}$$

The singular value shrinkage is applied to the singular values contained on the diagonal of $S$ as

$$S_{\lambda_1/\eta_1}(\delta\sigma^{c+1}) = \sum_{i=0}^{\min(m,n)} (\gamma_i - \mu\gamma_i/\eta_1)_+ u_i v_i^* \tag{17}$$

here, $u_i$, $v_i$ and $\gamma_i$ are the singular vectors and values of

$$(\gamma)_+ = \begin{cases} \gamma, & \text{if } \gamma \geq 0 \\ 0, & \text{else} \end{cases} \tag{18}$$

$\delta\sigma^{c+1}$, respectively. The thresholding function is defined as:

The solution to the third subproblem (14) requires the joint processing of all terms $Q(\delta\sigma^{c+1})$, such that the magnitude is reduced

$$S^{c+1} = \frac{Q(\delta\sigma^{c+1})}{\left\|Q(\delta\sigma^{c+1})\right\|_2^2} \cdot \left(\left\|Q(\delta\sigma^{c+1})\right\|_2^2 - \frac{\lambda_2}{\eta_2}\right)_+ = k_{\lambda_2/\eta_2}(\delta\sigma^{c+1}) \tag{19}$$

The convergence of the above three-step alternating minimization scheme as the penalty parameters $\eta_1, \eta_2 \to \infty$ is well known [17].

To summarize, regularized matrix recovery schemes as a constrained minimization problem using a variable splitting framework involves the following three step algorithm with a continuation strategy, as show in Table 1:

**TABLE 1. Variable splitting algorithm for solving low-rank plus sparse problem of EIT reconstruction.**

**Input:** EIT measured voltage- $\delta U$ , Sensitivity matrix- $J$ , $(\eta_1)_0, (\eta_2)_0 > 0$ , $R = 0$ , $S = 0, \delta\sigma_0 = J^T \delta U$ , Initial dictionary $D_0$ .

1) Obtain dictionary $D$ according to the equation (9);

2) Solve the equation (12) by using the CG scheme [20];

3) Solve equation (13) according to the result of equation (12);

4) Solve equation (14) according to the result of equation (13);

5) Repeat step 1-4 until the stopping criterion is defined as equation (11).

$$g_c = \left|\frac{G_{(\eta_1,\eta_2)}(\delta\sigma^c, R^c) - G_{(\eta_1,\eta_2)}(\delta\sigma^{c-1}, R^{c-1})}{G_{(\eta_1,\eta_2)}(\delta\sigma^c, R^c)}\right| < 10^{-6} \tag{20}$$

**Output**: $\delta\sigma$ - Multiple reconstructed conductivity distribution.

## IV. NUMERICAL EXPERIMENTS NUMERICAL SIMULATION

### A. SIMULATION MODEL

In this section, numerical simulations are implemented to evaluate the feasibility and effectiveness of the low-rank plus sparse algorithm. A mesh of adaptive first-order triangular elements produced in COMSOL Multiphysics is used for the forward calculation. The reconstructed images presenting conductivity distribution for inverse problem uses another mesh with 812 square elements to avoid the so-called ''inverse crime'' [2]. A 16-electrode round EIT sensor is used for simulations, and each frame is presented in 812 pixels. All algorithms are implemented using the MATLAB 2012 software on a PC with a 2.4 GHz CPU and 4 GB memory.

To evaluate the proposed reconstruction method, this paper takes the conductivity distribution shown in Fig.1 to obtain

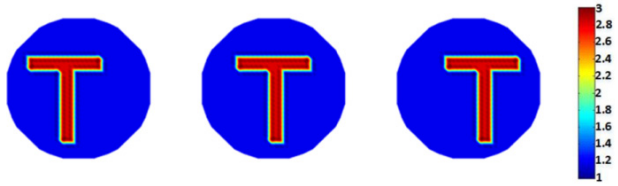

(a) T-shaped object

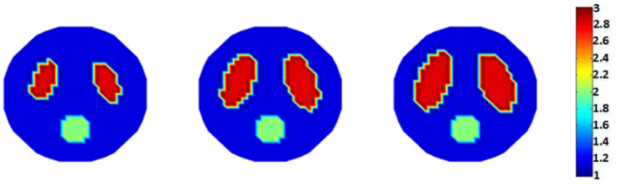

(b) Synthetic lung object

**FIGURE 1.** Simulated conductivity distribution. (a) T-shaped object, (b) Synthetic lung object (Unit of the color bar is conductivity value).

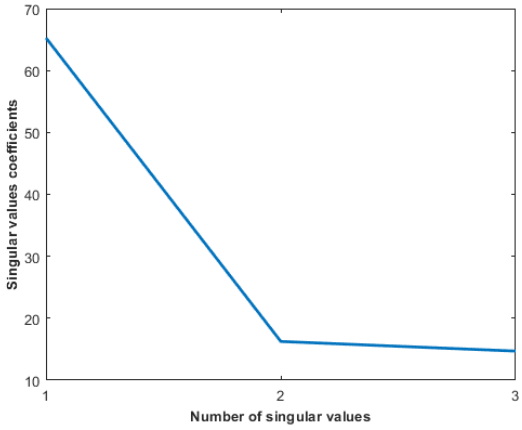


**FIGURE 2.** Decay of singular values of EIT data.

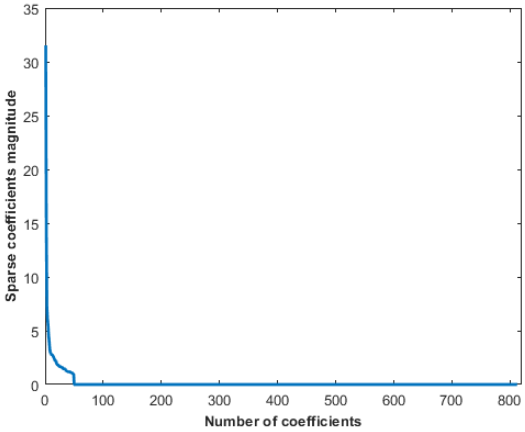


**FIGURE 3.** Sorted magnitude values of coefficients in transform domain.

simulation data for image reconstruction. Two conductivity variation phantoms, i.e. phantoms (a)-(b), are established. According to the noise level of the real system, the measured data with SNR = 42 dB are used for simulation.

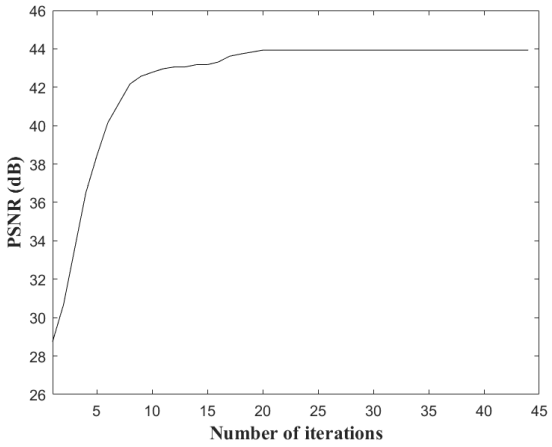


(a) Iteration curve for reconstruction of the T-shaped model

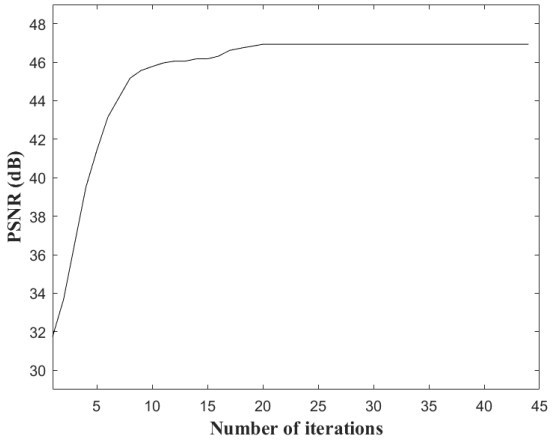


(b) Iteration curve for reconstruction of the synthetic lung model

**FIGURE 4.** The relationship between the PSNR of reconstructed image and the number of iterations for the low-rank plus sparse method.

The new method is first tested on simulation data collected with T-shaped object. An illustration is produced in Fig. 1 (a) to help explain the scheme. The example presents the reconstruction of images of a T-shaped object subject to translational displacements.

Another simulation is of the synthetic lung object, which is illustrated in Fig. 1 (b). The example extends the first simulation to the EIT images formed by ellipsoids of varying volume, which emulates the imaging of a breathing thorax.

### *B. EVALUATION OF LOW RANK AND SPARSITY PROPERTY FOR EIT IMAGE*

Since the low rank and sparse assumption are used this paper, the low-rankness and sparseness of the target process are proved first.

Firstly, the spatial-temporal conductivity matrix $\delta\sigma$ is assumed to be low rank. In order to show the validity of this assumption, we plot the sorted singular values of EIT spatial-temporal conductivity matrix $\delta\sigma$ corresponding to the conductivity distribution of synthetic lung object in Figure 1(b).

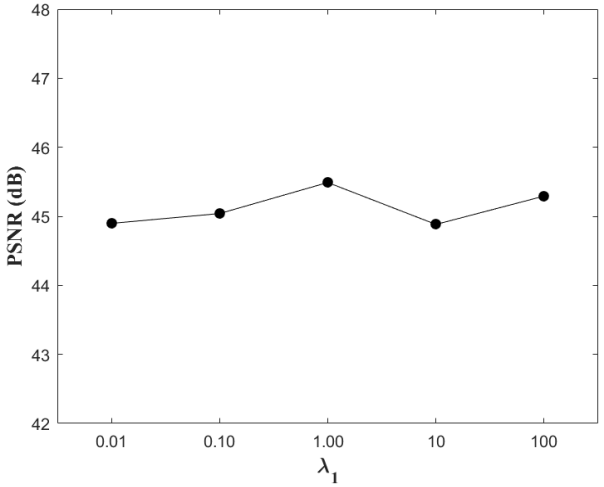


(a) Evaluation of $\lambda_1$ for reconstruction of the T-shaped model

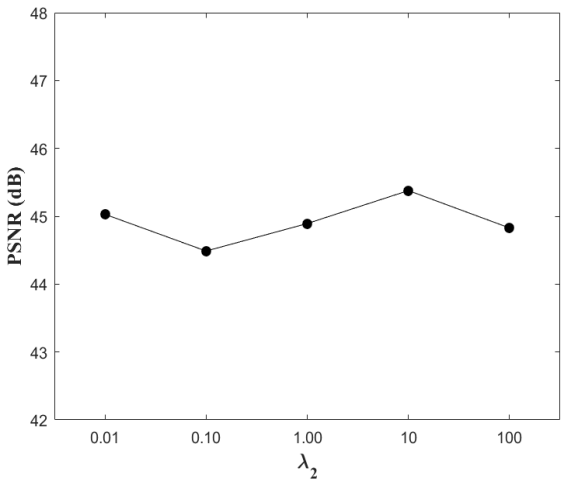


(b) Evaluation of $\lambda_2$ for reconstruction of the T-shaped model

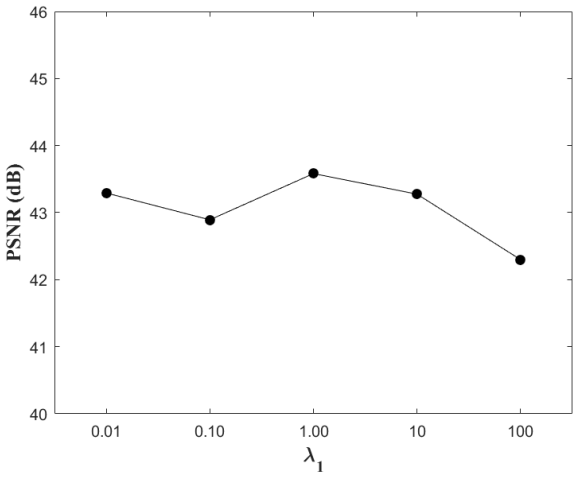


(c) Evaluation of $\lambda_1$ for reconstruction of the synthetic lung model

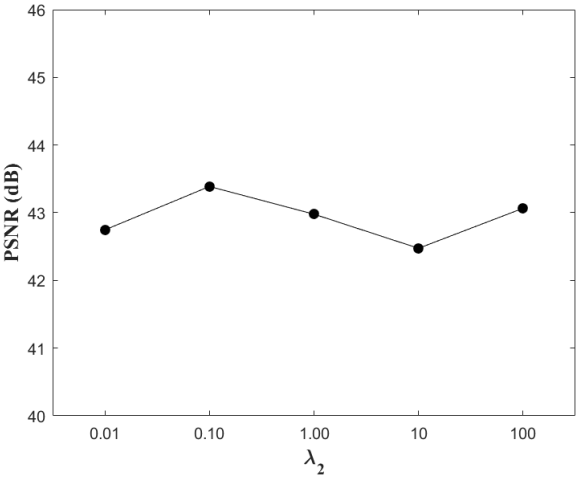


(d) Evaluation of $\lambda_2$ for reconstruction of the synthetic lung model

**FIGURE 5.** The relationship between the PSNR of reconstructed image and the regularization parameters for the low-rank plus sparse method.

The rapid decay of sorted singular values in Fig. 2 indeed confirms the low rank nature of dynamic EIT data.

Although the sparse property cannot be guaranteed by EIT image, it could be imposed on the transform domain data. Since the patch-based sparsity based on dictionary learning is used in this paper, we plot the sorted sparse coefficients of conductivity distribution corresponding to the middle phantom of Figure 1(b), as shown in Fig. 3. $7 \times 7$ square patch is used for sparse representation in this paper. We could observe that the EIT image is sparse under the condition of patch-based sparsity.

### C. EVALUATION PROCEDURE

To evaluate the properties of the low-rank plus sparse method, strategies for parameter choice are discussed based on the simulation results. The peak signal-to-noise ratio (PSNR) and the average structural similarity (MSSIM) parameters are selected for evaluation of image quality [21]–[24].

a) The quality of the reconstruction is quantified by using the peak signal-to-noise ratio (PSNR):

$$PSNR = 10^* \log_{10}\left(\frac{(2^n - I)^2}{MSE}\right) \tag{21}$$

where

$$MSE = \frac{1}{n}\sum_{i=0}^{n-1} \|I(i) - K(i)\|_2^2 \tag{22}$$

represents the mean square error. $I$ and $K$ represent real image $I(i)$ and reconstructed image $K(i)$ respectively. $i$ is the index of a pixel in each image.

b) The structural similarity index (SSIM) evaluation models is used to obtain the comprehensive evaluation index of the image quality by comparing the difference between the original image and the distortion images in the three categories of brightness, contrast and structure.

$$SSIM(x, y) = [w(x, y)]^{\alpha}[c(x, y)]^{\beta}[s(x, y)]^{\gamma} \tag{23}$$

**TABLE 2. Dimensions of nylon rods tested at different times.**

| time | | t1 | t2 | t3 | t4 | t5 | t6 | t7 | t8 |
|---|---|---|---|---|---|---|---|---|---|
| Size (cm) | minor axis | 3 | 2 | 1.5 | 1 | 1 | 1.5 | 2 | 3 |
| | long axis | 4 | 3 | 2 | 1.5 | 1.5 | 2 | 3 | 4 |

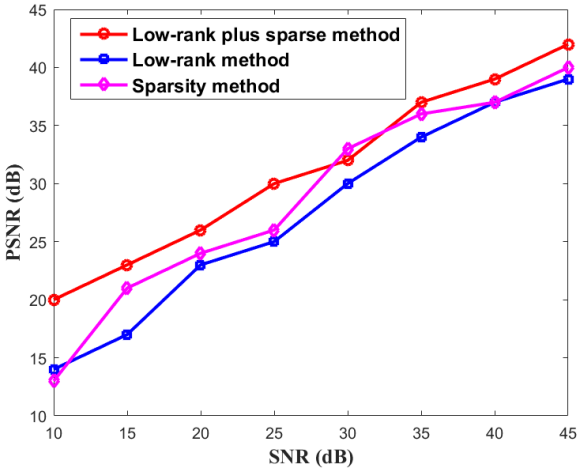


(a) The parameter PSNR of the T-shaped model

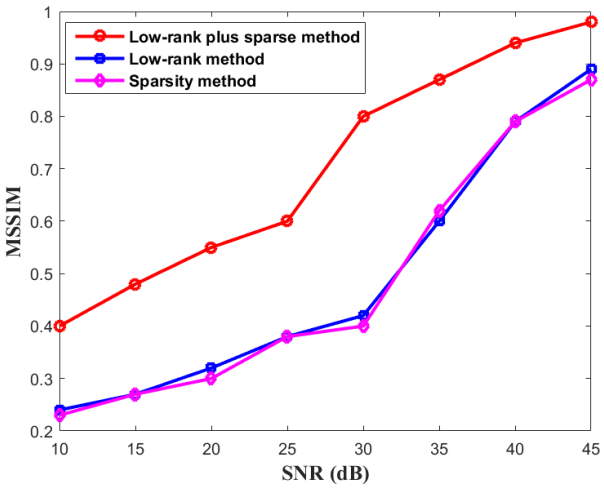


(b) The parameter MSSIM of the T-shaped model

**FIGURE 6. Comprehensive quantitative image quality evaluation of reconstruction of the T-shaped model with different SNRs.**

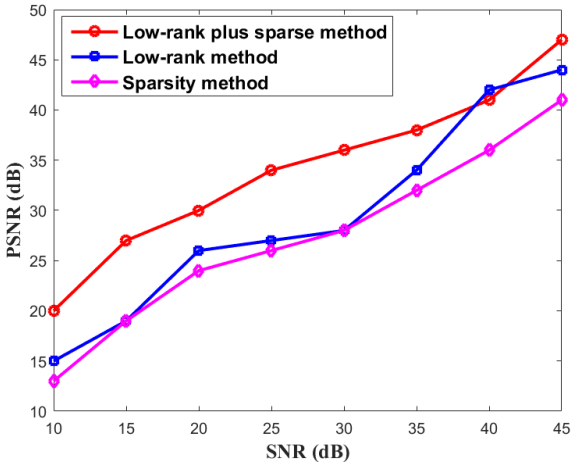


(a) The parameter PSNR of the synthetic lung model

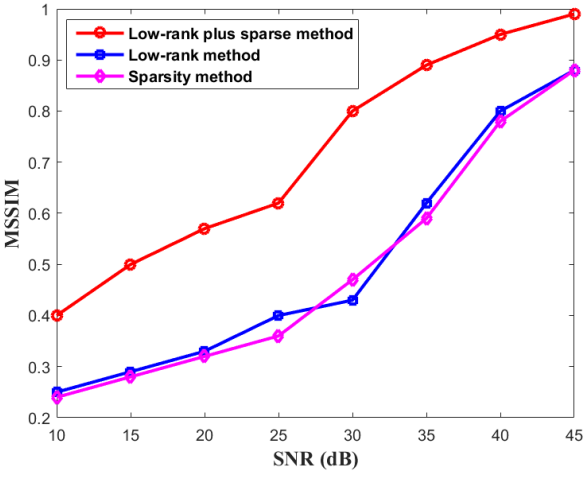


(b) The parameter MSSIM of the synthetic lung model

**FIGURE 7. Comprehensive quantitative image quality evaluation of reconstruction of the synthetic lung model with different SNRs.**

where $w(x, y) = \frac{2u_x u_y + C_1}{u_x^2 + u_y^2 + C_1}$, $c(x, y) = \frac{2\sigma_x \sigma_y + C_2}{\sigma_x^2 + \sigma_y^2 + C_2}$ and $s(x, y) = \frac{\sigma_{xy} + C_3}{\sigma_x \sigma_y + C_3}$ are brightness message information, contrast message information and structure message information of the image, respectively. $x$ and $y$ represent the standard image and the image to be evaluated, respectively. $u_x$ and $u_y$ denote the mean value of the image. $\sigma_x$ and $\sigma_y$ denote the standard deviation of the image. $\sigma_{xy}$ denotes the covariance of the image. $C_1 = (k_1 * L)^2$, $C_2 = (k_2 * L)^2$ and $C_3 = C_2/2$ are constant to keep the denominator from being zero (In this paper, $k_1 = 0.01, k_2 = 0.03, L = 255$).The choice are $\alpha = 1$, $\beta = 1$ and $\gamma = 1$.

The obtained SSIM values were accumulatively averaged, and the average structural similarity MSSIM of the two images was defined as:

$$MSSIM = \frac{1}{M} \sum_{i=1}^{M} SSIM(x_i, y_i) \tag{24}$$

where $M$ represents the number of local window openings. $x_i$ and $y_i$ represent the $i$ local image of the standard image and the image to be evaluated, respectively.

#### 1) ITERATION NUMBER SELECTION

The variable splitting algorithm, which is an iterative algorithm, is used to solve the low-rank plus sparse method. The two conductivity distributions in Fig. 1 were reconstructed by the low-rank plus sparse method with 45 iterations. The plots of the PSNR defined in equation (21) versus iterative steps are calculated and shown in Fig.2. For the low-rank plus sparse method, the regularization parameter $\lambda_1$ and $\lambda_2$ are both selected as 0.1, respectively. The initial value of $\delta\sigma$ is 0.

It can be seen from Fig. 4 that the PSNR parameter increases slowly after 20 iterative steps for both models. Considering both the image quality and the computing efficiency, the iteration number is selected as 20 in this paper.

#### 2) REGULARIZATION PARAMETER

The regularization parameter $\lambda_1$ and $\lambda_2$ are important to determine the weight of the regularization.

The influence of different regularization parameters on PSNR of the reconstructed image is shown in Fig. 5. It can be seen from Fig. 5 that the quality of the reconstructed images does not obviously changes in the regularization parameters $\lambda_1$ and $\lambda_2$, which indicates that the selection of the regularization parameter $\lambda_1$ and $\lambda_2$ has little effect on the image quality.

#### 3) EVALUATION OF THE NEW METHOD CONSIDERING SYSTEM NOISE

In actual measurements, the detected data contain a large number of noise signals. To test the noise robustness of the low-rank plus sparse method, different levels of White Gaussian noise are added to the measured data. The proposed method is compared with traditional methods, using both the evaluation parameters and reconstructed images.

In Figs. 6 and 7, both PSNR and MSSIM were used to evaluate the reconstruction results of different methods for a variety of system SNRs. As shown in Fig. 4 and 5, the low-rank plus sparse method is particularly robust to noise pollution, even at a high noise level and when the SNR is below 20 dB.

Reconstructed images of the measured data under practical system noise conditions (SNR = 42 dB) are shown in Fig. 8. For the convenience of comparison, the gray levels of the reconstructed images are normalized to the range of 1 to 3. As shown in Fig. 8, the quality of reconstructed images based on low rank and sparse algorithms are similar. This is because the spatial and temporal noise are not considered very well in traditional methods. Hence the artifacts with similar characteristics according to system noise are introduced. However, the performance of reconstruction is significantly improved after combination of both low rank and sparse constraint.

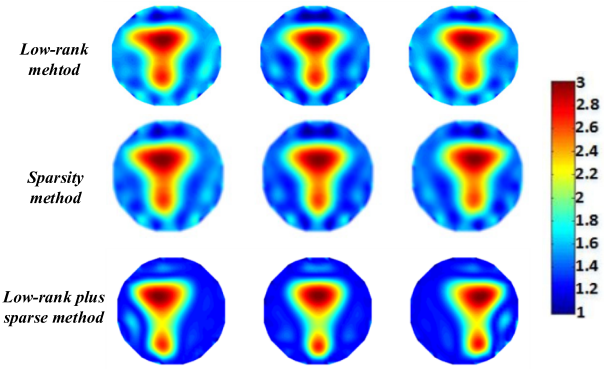


(a) Reconstucted images for the T-shaped model

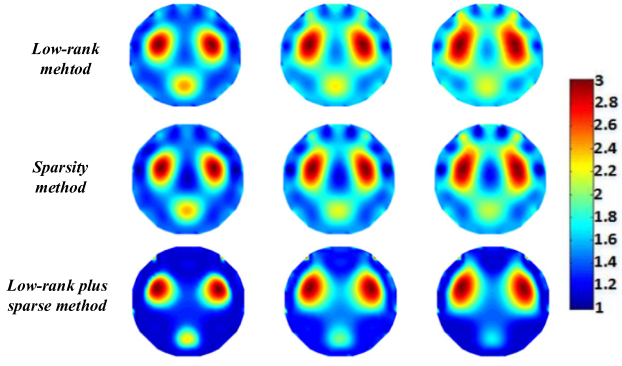


(b) Reconstucted images for the synthetic lung model

**FIGURE 8.** Reconstructed images based on the three methods fort the two simulation models (Unit of the color bar is conductivity value).

## V. EXPERIMENTAL RESULT

An experimental study is performed using a measurement setup, as shown in Fig. 9. Sixteen composite electrodes are evenly distributed on the inner surface of the container. Consistent with the simulation study in section IV, the 16-electrode sensor is used in the experiment. The adjacent current injection and voltage measurement strategy is adopted, and the amplitude data of the boundary voltage

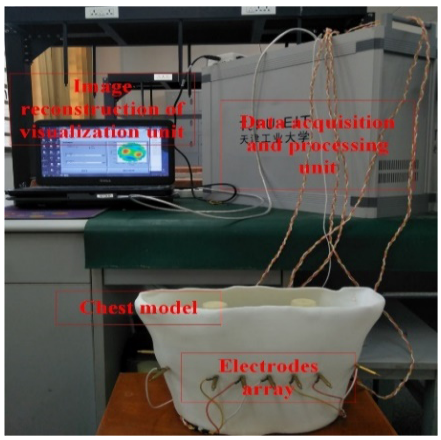


**FIGURE 9.** Experimental equipment for thoracic cavity model imaging.

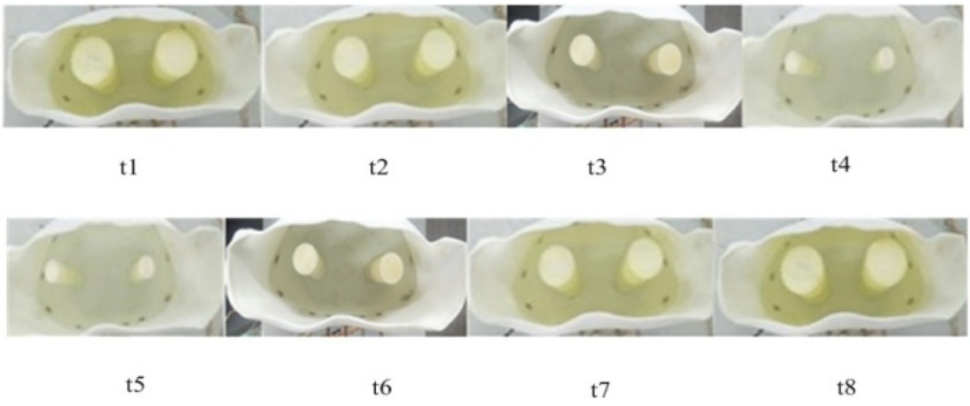


**FIGURE 10.** Experimental configurations representing human body lung ventilation.

measurement strategy is the voltage that is acquired for image reconstruction. In the data acquisition and control system, the AC-based sensing electronics are composed of a resistor voltage (R/V) converter and an AC programmable gain amplifier (AC-PGA). The digital signals are captured and processed by the FPGA (Xilinx Spartan-3XC3S400), including digital phase sensitive demodulation (digital PSD) and first-in, first-out (FIFO). The maximum current amplitude of the adjacent electrode current excitation mode is 0.2 mA. All measurements are made at 3 kHZ. The SNR of the system is 42 dB. The data acquisition speed of the system is approximately 30 frames/s.

To simulate the changes of pulmonary ventilation during the process of breathing, four sizes of well-trimmed rods are positioned in a chest model, as shown in Fig. 10. The top surface of the chest model is 28.9 cm in length and 9 cm in width; the bottom surface of the chest model is 20cm in length and 13.5 cm in width. We fill the model with saline water with conductivity of $0.3Sm^{-1}$, according to the conductivity of tissue fluid. In addition, we include nylon rods in large, medium and small sizes so that we can simulate the size change during lung ventilation. The conductivity of nylon rods is $0.1Sm^{-1}$, according to the conductivity of the lung tissue. Detail information on these sizes of nylon rods is shown in Table 2. Each space-time volume in a specific time window contains 8 frames, i.e., $\delta\Sigma \in R^{812\times 8}$ and $\delta U \in R^{208\times 8}$.

The experimental imaging results based on the low-rank method, sparsity method and low-rank plus sparse method are shown in Fig. 11. The gray levels of the reconstructed images are normalized to the range of 1 to 3 for convenient comparison. Both the PSNR and MSSIM parameters of the reconstructed images are calculated. Although the low-rank method and sparsity method capture the main motion feature, they lose some local contrast. As we can see, the proposed method achieves the highest PSNR among the three methods. This proves that we achieved a better sparsity constraint for EIT reconstruction with the patch-based sparse representation based on dictionary learning.

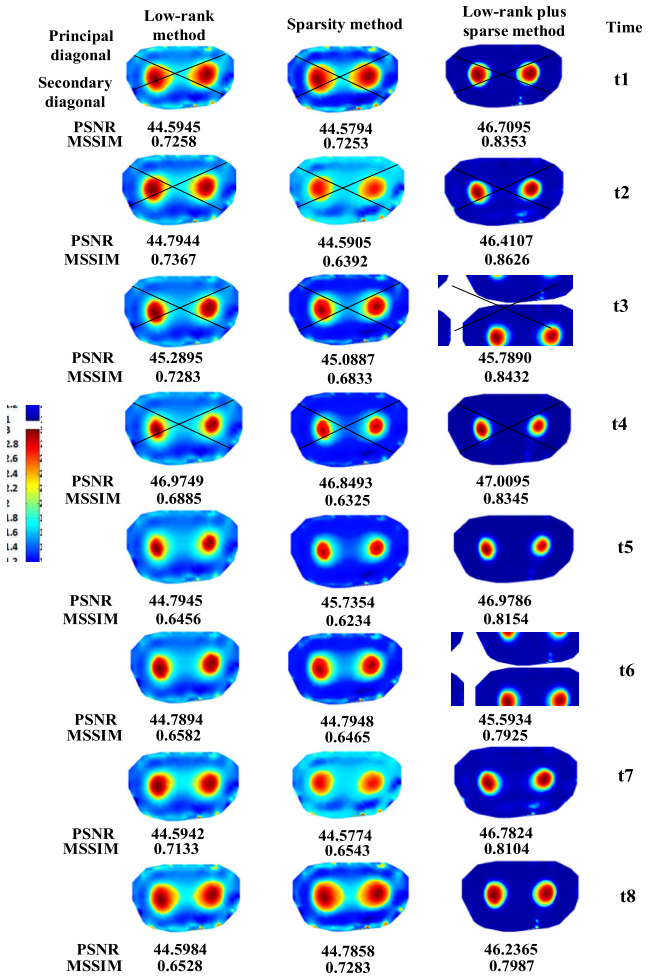


**FIGURE 11.** Reconstruction results for the 2D lung phantom experiment.

According to the MSSIM parameters for the change of lung ventilation during the breathing process, the proposed method achieves better structural similarity to ground truth than do other methods.

The edge features of image reconstructed by different algorithms are tested and compared. The comparison of

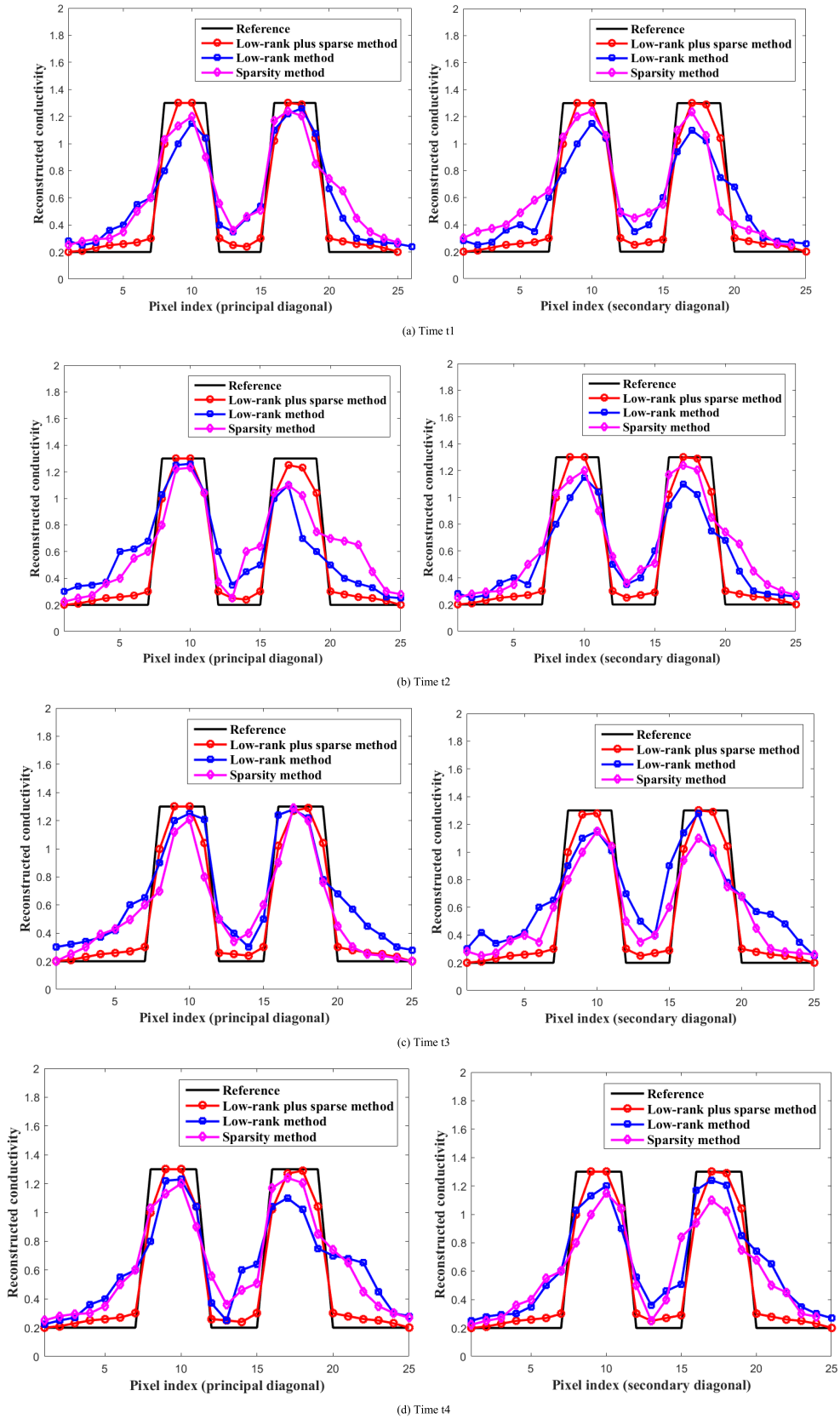


**FIGURE 12.** Conductivity distribution of the1D profiles diagonally through the reference images and reconstructed versions generated by the low-rank plus sparse method, low-rank method and sparsity method.

reconstructed conductivity profile of the solid black line in Fig.9 (t1-t4) is shown in Fig.12. Compared with other methods, the low-rank plus sparse method based on patch-based sparsity shows similarly good retention of the mutation features and edge definition. The image artifacts of the new method are also reduced. The advantage is further confirmed by the 1D profiles diagonally through the reference and reconstructed images. It can be observed that the low-rank plus sparse method yields reconstructions with 1D diagonal files that are more structurally similar to the reference image than those of the other methods.

## VI. CONCLUSION

A low-rank plus sparse scheme is proposed for dynamic EIT reconstruction. The patch-based sparse strategy is used for sparse representation of an EIT image with an irregular boundary. The strategies for parameter selection and the robustness of the new method are discussed. Both the simulation and experimental results shown that the low-rank plus sparse method provides obviously superior quality of the reconstructed images compared with the low-rank method and the sparse method and has the potential for use to monitor the pulmonary ventilation process.

In future work, 3D EIT images will be reconstructed under the framework of compressive sensing to improve real-time performance for dynamic EIT reconstruction. Furthermore, the fusion of EIT and CT reconstruction will be studied as an approach to combine functional and structural information for the promotion of medical imaging technology.

## REFERENCES

[1] Q. Wang, H. Wang, Z. Gui, and C. Yang, "Reconstruction of electrical impedance tomography (EIT) images based on the expectation maximum (EM) method," *ISA Trans.*, vol. 51, pp. 808–820, Nov. 2012.

[2] M. Hanke and M. Brühl, "Recent progress in electrical impedance tomography," *Inverse Probl.*, vol. 19, no. 6, pp. S65–S90, 2003.

[3] D. Isaacson, J. L. Mueller, J. C. Newell, and S. Siltanen, "Reconstructions of chest phantoms by the D-bar method for electrical impedance tomography," *IEEE Trans. Med. Imag.*, vol. 23, no. 7, pp. 821–828, Jul. 2004.

[4] M. Cheney, D. Isaacson, and J. C. Newell, "Electrical impedance tomography," *SIAM Rev.*, vol. 41, no. 1, pp. 85–101, 1999.

[5] T. Strauss, "Statistical inverse problems in electrical impedance and diffuse optical tomography," Ph.D. dissertation, Dept. ProQuest Diss. Theses Global, Clemson Univ., Clemson, SC, USA, 2015.

[6] Q. Wang, Y. Peng, X. Chen, J. He, P. Zhang, J. Wang, R. Zhang, and H. Wang, "Dynamic imaging based on spatio-temporal information for electrical impedance tomography," in *Proc. IEEE Int. Instrum. Meas. Technol. Conf. (IMTC)*, May 2017, pp. 1–5.

[7] J. Ye, H. Wang, and W. Yang, "Image recovery for electrical capacitance tomography based on low-rank decomposition," *IEEE Trans. Instrum. Meas.*, vol. 66, no. 7, pp. 1751–1759, Jul. 2017.

[8] Q. Wang, P. Zhang, J. Wang, Q. Chen, Z. Lian, X. Li, Y. Sun, X. Duan, Z. Cui, B. Sun, and H. Wang, "Patch-based sparse reconstruction for electrical impedance tomography," *Sensor Rev.*, vol. 37, no. 3, pp. 257–269, Jun. 2017.

[9] B. Jin, T. Khan, and P. Maass, "A reconstruction algorithm for electrical impedance tomography based on sparsity regularization," *Int. J. Numer. Methods Eng.*, vol. 89, no. 3, pp. 337–353, Jan. 2012.

[10] S. Liu, J. Jia, Y. D. Zhang, and Y. Yang, "Image reconstruction in electrical impedance tomography based on structure-aware sparse Bayesian learning," *IEEE Trans. Med. Imag.*, vol. 37, no. 9, pp. 2090–2102, Sep. 2018.

[11] T. Strauss and T. Khan, "Statistical inversion in electrical impedance tomography using mixed total variation and non-convex $\ell_p$ regularization prior," *J. Inverse Ill-Posed Probl.*, vol. 23, no. 5, pp. 529–542, May 2015.

[12] P. Wang, Q. Chen, and N. Shao, "Moving object detection via low-rank total variation regularization," *Proc. SPIE*, vol. 9971, Sep. 2016, Art. no. 997132.

[13] J. Yang, Y. Zhang, and W. Yin, "A fast alternating direction method for TVL1-L2 signal reconstruction from partial Fourier data," *IEEE J. Sel. Topics Signal Process.*, vol. 4, no. 2, pp. 288–297, 2010.

[14] J. Wang, J. Ma, B. Ho, and Q. Li, "Split Bregman iterative algorithm for sparse reconstruction of electrical impedance tomography," *Signal Process.*, vol. 92, no. 12, pp. 2952–2961, Dec. 2012.

[15] J. Yang and Y. Zhang, "Alternating direction algorithms for $\ell_1$-problems in compressive sensing," *SIAM J. Sci. Comput.*, vol. 33, no. 1, pp. 250–278, 2009.

[16] S. Boyd, N. Parikh, E. Chu, B. Peleato, and J. Eckstein, "Distributed optimization and statistical learning via the alternating direction method of multipliers," *Found. Trends Mach. Learn.*, vol. 3, no. 1, pp. 1–122, Jan. 2011.

[17] S. G. Lingala, Y. Hu, E. DiBella, and M. Jacob, "Accelerated dynamic MRI exploiting sparsity and low-rank structure: $\kappa$-t SLR," *IEEE Trans. Med. Imag.*, vol. 30, no. 5, pp. 1042–1054, May 2011.

[18] R. Otazo, E. J. Candès, and D. K. Sodickson, "Low-rank plus sparse matrix decomposition for accelerated dynamic MRI with separation of background and dynamic components," *Magn. Reson. Med.*, vol. 73, no. 3, pp. 1125–1136, 2014.

[19] M. Aharon, M. Elad, and A. Bruckstein, "K-SVD: An algorithm for designing overcomplete dictionaries for sparse representation," *IEEE Trans. Signal Process*, vol. 54, no. 11, pp. 4311–4322, Oct. 2006.

[20] H. Zhu, Y. Xiao, and S.-Y. Wu, "Large sparse signal recovery by conjugate gradient algorithm based on smoothing technique," *Comput. Math. Appl.*, vol. 66, pp. 24–32, Aug. 2013.

[21] Y. Sun, L. Zhang, T. Fei, and X. Liu, "Variational Bayesian blind restoration reconstruction based on shear wave transform for low-dose medical CT image," *EURASIP J. Image Video Process.*, vol. 2017, no. 1, Oct. 2017, Art. no. 84.

[22] J. Zhang, Y. Sun, Y. Zhang, and J. Teng, "Double regularization medical CT image blind restoration reconstruction based on proximal alternating direction method of multipliers," *EURASIP J. Image Video Precess.*, vol. 2017, no. 1, Oct. 2017, Art. no. 70.

[23] S. Park, S. Kim, B. Yi, G. Hugo, H. M. Gach, and Y. Motai, "A novel method of cone beam CT projection binning based on image registration," *IEEE Trans. Med. Image.*, vol. 36, no. 8, pp. 1733–1745, Aug. 2017.

[24] H. Haider, J. Ali, S. M. Qureshi, H. Omer, and K. Kadir, "Compressively sampled MRI recovery using modified iterative-reweighted least square method," *Appl. Magn. Reson.*, vol. 47, no. 9, pp. 1033–1046, Sep. 2016.

**QI WANG** received the B.S. degree in automation, the M.S. degree in measurement technology and automatic devices, and the Ph.D. degree in engineering from Tianjin University, Tianjin, China, in 2007, 2009, and 2012, respectively.

Since 2012, she has been engaged in scientific research and teaching with the School of Electronics and Information Engineering, Tianjin Polytechnic University, where she is currently an Associate Professor. She has published more than 30 academic articles in important academic journals and conferences at home and abroad, and more than two inventions. Her current research interests include medical imaging, process tomography, and intelligent information processing.

**FEI LI** received the B.S. degree in engineering from the Huihua College, Hebei Normal University, in 2017. She is currently pursuing the M.S. degree with the School of Electronics and Information Engineering, Tianjin Polytechnic University.

**JIANMING WANG** received the B.S. degree in electrical engineering from the Hebei University of Technology, Hebei, China, in 1997, and the M.S. degree in mechanics and the Ph.D. degree in electrical and automation engineering from Tianjin University, Tianjin, China, in 2000 and 2003, respectively.

Since 2003, he has been engaged in scientific research and teaching with the School of Electronics and Information Engineering, Tianjin Polytechnic University, where he is currently a Professor. His current research interests include computer vision and intelligent information processing technology.

**XIAOJIE DUAN** received the B.S. degree from the School of Information Engineering and the M.S. degree from the School of Information Engineering, Hebei University of Technology, Hebei, China, in 2003 and 2006, respectively, and the Ph.D. degree from the State Key Laboratory of Precision Testing Technology and Instrument, Tianjin University, Tianjin, China, in 2013.

Since 2013, he has been engaged in scientific research and teaching with the School of Electronics and Information Engineering, Tianjin Polytechnic University, where he is currently an Associate Professor. His current research interests include digital image processing and electronic-optical detection technology.

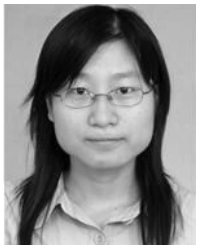

**XIUYAN LI** received the B.S. degree in information science and engineering from the Hebei University of Science and Technology, Hebei, China, in 2003, the M.S. degree in information science and engineering from the Hebei University of Technology, Hebei, in 2007, and the Ph.D. degree from the State Key Laboratory of Precision Testing Technology and Instrument, Tianjin University, Tianjin, China, in 2010.

Since 2010, she has been engaged in scientific research and teaching with the School of Electronics and Information Engineering, Tianjin Polytechnic University, where she is currently a Lecturer. As the first author, she has published more than ten academic articles in important academic journals and conferences at home and abroad. Her current research interests include computer vision, pattern recognition, and optic-electronic detection techniques.